1 **Supplementary Information for:** Phylogenomics of bonytongue fishes (Osteoglossomorpha)

2 shed light on the craniofacial evolution and biogeography of the weakly electric clade

3 (Mormyridae)

4 Rose D. Peterson[1], John P. Sullivan[3], Carl D. Hopkins[3], Aintzane Santaquiteria [4], Casey B.

5 Dillman[3], Stacy Pirro[5], Ricardo Betancur-R[4], Dahiana Arcila[4,6], Lily C. Hughes[7], Guillermo

6 Ortí[1,2].

7 [1]Department of Biological Sciences, The George Washington University, Washington,

8 DC USA [2]National Museum of Natural History, Smithsonian Institution, Washington,

9 DC USA

10 [3]Cornell University Museum of Vertebrates, Department of Ecology and Evolutionary

11 Biology Ithaca, NY USA

12 [4] Department of Biology, University of Oklahoma, Norman, OK USA

13 [5] Iridian Genomes Inc., Bethesda, MD USA

14 [6] Department of Ichthyology, Sam Noble Oklahoma Museum of Natural History,

15 Norman, OK, USA

16 [7] Department of Organismal Biology and Anatomy, University of Chicago, Chicago, IL

17 USA.

18

19 This file contains:

20 SUPPLEMENTARY METHODS

21 *DNA Extraction and Sequencing*

22 *Quality Control, Sequence Assembly, and Alignments*

23 *Divergence-time Estimation and Fossil calibrations*

33

34

35   SUPPLEMENTARY METHODS

36

37 ***DNA Extraction and Sequencing***.— We extracted genomic DNA from muscle or fin clips at the

38 Laboratory of Analytical Biology, Smithsonian Institution National Museum of Natural History.

39 Extractions followed the standard animal tissue phenol protocol for the Gene Prep (Autogen)

40 platform. We eluted DNA extracts in 50 microliters of Autogen R9 Buffer and assessed the

41 quality of DNA by visual inspection in a 1% agarose gel. DNAs of high quality were dried using

42 an Eppendorf Vacufuge and 153 samples were shipped to Arbor BioSciences in Ann Arbor,

43 Michigan, for library preparation. Genomic libraries were enriched for exons using the dual-

44 round ("touchdown") target capture protocol of Li et al. (2013) with eight samples multiplexed

45 per hybridization reaction. We used the "Backbone 1" probe set to enrich libraries for a set of

46 1,105 target exons defined by Hughes et al. (2020). Enriched libraries were pooled and

47   sequenced at the University of Chicago Genomic facility on a HiSeq 4000 lane with paired-end

48   150 bp reads.

49   In addition to the 153 individuals used for the exon-capture protocol, 44 additional taxa

50   that spanned the morphological diversity among species in the family Mormyridae and other

51   osteoglossomorphs were chosen for whole genome sequencing (Supplementary Table S1).

52   Tissue samples for these taxa were shipped to GeneWiz in South Plainfield, New Jersey, for

53   DNA extraction, library preparation, and sequencing. Genomic DNA was extracted with a

54   Qiagen DNeasy Kit and quality was visually assessed for the presence of high molecular weight

55   bands in a 1% agarose gel. Library preparation was performed with an Illumina TruSeq Kit on a

56   size-selected pool of 600 bp fragments; these libraries were "shotgun" sequenced on an Illumina

57   HiSeq X Ten, producing 150 bp paired-end reads (multiplexed five samples per lane).

58

59   *Quality Control, Sequence Assembly, and Alignments.*— Following the bioinformatics pipeline

60   described in Hughes et al. (2020), we used Trimmomatic v0.36 (Bolger et al. 2014) to filter the

61   raw FASTQ file, eliminating adapter contamination, low-quality bases (Phred score < 33) and

62   short reads (< 31bp). We mapped trimmed reads against a master file (FASTA format, Hughes et

63   al. 2020) containing all sequences used for probe design with BWA-MEM v0.7.17 (Li and

64   Durbin 2009). Next, we ran SAMtools v1.10 (Li et al. 2009) to remove PCR duplicates and sort

65   reads that mapped to each exon. For each species, we used Velvet v1.2.10 (Zerbino and Birney

66   2008) to obtain an initial assembly for each exon. The longest contig produced in Velvet served

67   as the initial reference sequence for input to aTRAMv2.0 (Allen et al. 2018) that was run with

68   five iterations to extend contigs with Trinity v2.8.5 (Grabherr et al. 2013) as the chosen

69   assembler. Each new iteration updates the reference sequence to the longest contig produced in

70   the previous iteration. Redundant contigs produced by aTRAM with 100% similarity were

71   removed with CD-HIT v4.6 (Li and Godzik 2006). Open reading frames for the contigs were

72   identified and extracted with Exonerate v2.4.0 (Slater and Birney 2005); contigs without a

73   reading frame were removed. If a single contig contained the opening reading frame, the exon

74   was considered ready for multiple sequence alignment. If multiple contigs contained an open

75   reading frame and they had less than 99% similarity based on CD-HIT (i.e., they are unlikely to

76   represent allelic variation), they were excluded from downstream analyses. All sequences

77   assembled for each exon that passed the above criteria were aligned with MACSE v2.03

78   (Ranwez et al. 2018), a reading-frame aware aligner.

79   Mining target exons following the pipeline optimized by Hughes et al. (2018). HMMER

80   uses the multiple sequence alignments produced for each exon using the target-capture methods

81   (above), to first build Hidden Markov Model (HMM) profiles for each exon and then uses these

82   profiles to search for and report homologous fragments in the assembled genomes. Homologous

83   sequences are extracted and then placed into FASTA files for each exon using custom Python

84   scripts (Hughes et al., 2020). Finally, extracted exons are aligned together with exons obtained

85   via target capture exons using MACSE, as described above.

86   We filtered alignments for downstream analysis with three major criteria: missing data

87   (>50% missing sequences), non-monophyly of Mormyridae in gene trees, and the TreeShrink

88   algorithm (Mai and Mirarab 2018). We visually inspected gene trees to minimize the potential

89   effect of paralogous sequences and potential cases of cross-contamination, gene trees flagged by

90   CheckMonophyly.py (Hughes et al. 2020) when the family Mormyridae was not monophyletic.

91   This family was chosen as a 'flag' since multiple lines of evidence strongly supported its

92   monophyly. Misplaced taxa, or the complete exon alignment, were excluded from downstream

93   analysis after visual inspection. TreeShrink was used to remove sequences from alignments and

94   gene trees.

95   ***Divergence-time Estimation and Fossil Calibrations.***—Description of fossil data, secondary

96   calibrations, and priors used in the analysis.

97   **Secondary Calibration 1**: Root, Crown Neopterygii (Betancur et al., 2013; Hughes et

98   al., 2018; Broughton et al., 2013; Giles et al., 2017). Maximum and minimum ages used as a

99   prior for this node represent the range of values reported by these studies. Calibration prior for

100 MCMCTree: B(300,328,0.025,0.025), applied to node 1 in Figure 1E.

101 **Secondary Calibration 2**: Teleostei, Crown teleosts (Betancur et al., 2013; Hughes et

102 al., 2018; Broughton et al., 2013; Giles et al., 2017). Maximum and minimum ages used as a

103 prior for this node represent the range of values reported by these studies. Calibration prior for

104 MCMCTree: B(249,284,0.025,0.025), applied to node 2 in Figure 1E.

105 **Secondary Calibration 3**: Elopomorpha, Crown elopomorphs, the most recent common

106 ancestor (MRCA) of Megalops and Anguilla. (Betancur et al., 2013; Hughes et al., 2018;

107 Broughton et al., 2013). Maximum and minimum ages used as a prior for this node represent the

108 range of values reported by these studies. Calibration prior for MCMCTree: B(180,215,

109 0.025,0.025), applied to node 3 in Figure 1E.

110 **Fossil 1**: MCRA *Hiodon alosoides* and *Hiodon terisus.* Hard lower bound: †*Eohiodon*

111 (Wilson 1978); Hilton and Grande 2008). Diagnosis and placement: Due to a lack of characters

112 that are able to distinguish *Hiodon* from †*Eohiodon* they should be considered synonymous

113 (Hilton and Grande 2008). Therefore, due to *Hiodon* and †*Eohiodon* being synonymous we

114 treated is as crow calibration point for MCRA *Hiodon alosoides* and *Hiodon terisus*. Age:

115 †*Eohiodon* is from the Eocene Klondike Mountain Formation, Tunnel Creek, and the Horsefly

116   Beds and Green River Formation. Paleogene, Eocene, Lutetian 45MY (47.8-41.3 MY) (Lavoué

117   2016) Calibration prior for MCMCTree: B(41.3,47.8,1e-300,0.05), applied to node a in Figure

118   1E.

119   **Fossil 2**: MCRA: *Arapaima* and *Heterotis.* Hard lower bound*: †Sinoglossus lushanensis*

120   (Su, 1986; Li and Wilson, 1996a) Diagnosis and placement: Closely related to *Arapaima* and

121   *Heterotis*, either as its sister group (Forey and Hilton, 2010; Li and Wilson, 1996b) or in a

122   trichotomy with *Heterotis* and *Arapaima* (Li and Wilson, 1996a; Lavoué, 2016; Wilson, Murray,

123   2008) based on the synapomorphies of the fusion of antorbital with first infraorbital and

124   reticulate scaled. Age: East Asia (freshwater), Paleogene, Eocene, Lutetian (41.3-47.8 MY.)

125   (Lavoué 2016). Therefore, we treated this fossil as crown calibration for *Arapaima* and

126   *Heterotis.* Calibration prior in MCMCTree: B(41.3,47.8,1e-300,0.05), applied to node b Figure

127   1E.

128   **Fossil 3**: MCRA: *Gymnarchus* and *Notopterus.* Hard lower bound: †*Palaeonotopterus*

129   *greenwoodi* (Forey 1997; Taverne and Maisey, 1999; Cavin and Forey 2001; Benton et al., 2015;

130   Lavoué 2016; Hilton and Lavoué, 2018). Diagnosis and placement: This fossil is considered a

131   stem mormyroid (Hilton 2003; Wilson and Murray 2008) but do to limitations with MCMCTree

132   is placed one node lower as MRCA *Gymnarchus* and *Notopterus*. Age: African Freshwater;

133   Upper Cretaceous, Cenomanian (93.9 - 100.5 MY) (Lavoué 2016). Calibration prior for

134   MCMCTree: B(93.9,100.5,1e-300,0.05), applied to node c in Figure 1E.

135   **Fossil 4**: MRCA: *Atractosteus, and Lepisosteus.* Hard lower bound: †*Atractosteus*

136   *falipoui* (Benton et al., 2015). Diagnosis and placement: the monophyloy of Atractosteus is

137   supported by the shape of vomerine heads, medical curvatures and expaspions on the anterior

138   coronoid and the absence of toothplates on the second and third hypobranchials (Grande 2010).

139 Therefore, we treated this fossil as a crown *Atractosteus*. Age: Africa, Upper Cretaceous

140 Cenomanian (100.5-93.9 Ma.). Calibration point for crown Lepisosteiformes (*MRCA of*

141 *Atractosteus, and Lepisosteus*). Calibration prior for MCMCTree: B(93.9,145,1e-300,0.05),

142 applied to node d in Figure 1e.

143   Due to redescriptions or phylogenetic uncertainties we choose to not include the

144 following fossils in our analyses: †*Joffrichthys* is no longer considered a member of

145 Osteoglossidae and †*Ostariostoma* may be allied to Gonorhynciformes (Murray et al. 2018). We

146 did not include †*Singida* or †*Chauliopareion* because of their uncertain affinities within

147 osteoglossomorphs (Hilton 2003; Murray and Wilson 2005; Bonde 2008; Xu and Chang 2009;

148 Forey and Hilton 2010; Murray et al. 2018).

149   Two partitions were implemented in MCMCTree for all molecular data sets (1-10 and

150 full dataset) by grouping all first and second codon positions into one and the third codon

151 positions to the other and assigned separate HKY substitution models for each. Although model-

152 testing in IQ-TREE (see above) indicated GTR as the best fitting model, this model is not

153 available in MCMCTree; therefore, we assigned HKY + gamma substitution models, the most

154 complex model available in MCMCTree. The MCMC chain was run independently for 4.5

155 million generations using a Birth-Death Process model and independent clock rates for subsets 1-

156 10. Further, for priors we implemented a burnin of 2000, a sampling frequency of 100, a birth

157 rate of 1, death rate of 1, and sampling of 0.27. Analysis of the complete dataset followed the

158 same process as the subsets but the MCMC chain was run for 7.5 million generations due to the

159 larger size of the data matrix and had a burnin of 2500. Log files for each analysis were assessed

160 for convergence with Tracer v1.8.4 (Rambaut et al. 2018), requiring ESS values >200 for all

161 parameters.

162   In order to further assess the trans-oceanic or vicariance biogeographic hypotheses for the

163   family Osteoglossidae that includes *Scleropages* (SE Asia and Australia) and *Osteoglossum* (S.

164   America) we considered an additional fossil, following recommendations from an anonymous

165   reviewer. The fossil †*Scleropages sinensis* is from the early Eocene Xiwanpu formation in

166   Hunan and the Yangxi Formation in Hubei, China is considered a crown *Scleropages* (Zhang and

167   Wilson 2017) and therefore was used to calibrate the *Osteoglossum + Scleropages* node. We

168   used the full dataset topologies inferred with IQ-TREE as the calibration trees and included all

169   the calibrations mentioned above in addition to the †*Scleropages sinensis* calibration

170   'B(48.6,55.8,1e-300,0.05)'. The priors, models, chain generations and burnin were the same as

171   mentioned above for the full dataset.

172

173   ***Biogeographic Analyses of Mormyridae.***— Mormyrids have a fragmentary fossil record

174   restricted to Africa and represented by skull bones, teeth or vertebrae (Greenwood 1972; Hilton

175   2003; Lavoué and Sullivan 2004; Wilson and Murray 2008; Lavoué et al. 2012; Lavoué 2016;

176   Hilton and Lavoué 2018). Extant mormyrids have a Pan-African distribution, occurring in seven

177   of nine ichthyofaunal provinces (Lévêque et al. 2008), and their species diversity is highest in the

178   Congo Basin. This pattern is also reported for other African freshwater fishes—e.g., the

179   characiforms Distichondontidae (*Distichodus,* Arroyave et al. 2020) and Alestidae *(Hydrocynus,*

180   Goodier et al. 2011)*,* the catfish Mochokidae (*Synodontis,* Day et al. 2013) and Amphiliidae

181   (FishBase, Froese and Pauly 2000), and the spiny eel Mastacembelidae (*Masatacembelus,* Day et

182   al. 2017)—and is consistent with an earlier hypothesis considering the Congo basin a source of

183   African fish diversity for more depauperate ichthyofaunal areas (Livingstone et al. 1982).

184   Palaeohydrological and paleoclimatic changes also have been suggested to promote

185   diversification of freshwater organisms (Lundberg 1998; Montoya-Burgos 2003). Increasing

186   temperatures and precipitation during the Middle Miocene Climatic Optimum ca. 17-15 Ma

187   (Flower and Kennett 1994; Zachos et al. 2001) may have caused swelling river flow discharge

188   and multiple connections between river basins. Western and Eastern Africa also were subject to

189   widespread uplift during the Miocene significantly shaping the current hydrological landscape

190   (Lavier et al. 2001; Sepulchre et al. 2006) a process that has been associated to increased

191   speciation in freshwater fishes and crabs (Day et al. 2013; Daniels et al. 2015; Arroyave et al.

192   2020). Africa has a rich ichthyofaunal diversity, but the patterns and processes responsible for

193   this diversity are poorly understood (Lévêque & Paugy 2017; Arroyave et al. 2020).

194   For each dispersal scheme, we tested 12 biogeographic models including the dispersal

195   extinction cladogenesis or "DEC" model (Ree and Smith 2008), the dispersal-vicariance or

196   "DIVA" model (Ronquist 1997), and the Bayesian inference of historical biogeography for

197   discrete areas or "BayAREA" model (Landis et al. 2013). Each model was run with and without

198   the j parameter to implement founder-speciation events (Matzke 2014) and with and without a

199   power exponential for the dispersal, or the w parameter (Dupin et al. 2017). The j parameter

200   allows for colonialization of a new area by a daughter lineage while the splitting-sister lineage

201   stays at the ancestral area and the w parameter infers the optimal dispersal matrix multiplier. The

202   w parameter was set to "free" to allow it to be optimized according to the data. The master tree

203   was used as the input phylogeny to independently calculate AIC scores for each biogeographic

204   model and for each dispersal scheme. The model with the best AIC was used for all subsequent

205   analyses. We accounted for phylogenetic uncertainty in topology and divergence-time estimates

206   based on trees inferred with independent evidence (complete datasets and subsets) and different

207   phylogenetic inference methods (ASTRAL or RAxML on the concatenated matrix), an approach

208 recently used for comparative and biogeographic inferences (Rincon-Sandoval et al. 2020;

209 Santaquiteria et al. 2021). In short, the biogeographic analyses (applying the best model) were

210 repeated using all 21 time-trees obtained in our study .To assess the effects of phylogenetic

211 variation in biogeographic inferences, we used a code produced by (Matzke 2019) to summarize

212 ancestral range estimates from multiple trees by selecting the "master tree" as the topology upon

213 which the results from all 21 trees were overlain. This approach allowed us to obtain averaged

214 probabilities across the different trees for compatible nodes present on the "master tree."

215

216   SUPPLEMENTARY RESULTS

217

218 *Data Set Properties.*—The exon-capture protocol was applied to 153 taxa, for which we

219 obtained an average of 1,239,212 reads per individual. Raw sequence data are available at NCBI

220 Bioproject (PRJNA699339). Assembly of raw reads into contigs for each of the 1,105 targeted

221 exons resulted in many sparsely populated alignments with less than 50% of the taxa. Low

222 target-capture efficiency of the "Backbone 1" probe set for osteoglossomorphs, and variable

223 quality of starting DNA may have led to failures to assemble exons for all taxa. Therefore, 566

224 exon alignments were excluded from downstream analysis. An additional 21 exons suspected of

225 containing paralogous sequences upon visual inspection of gene trees were removed. The

226 remaining 546 exons passed all quality control filters, had an average length of 445 bp

227 (concatenated length = 245,986 bp), and were used for all downstream phylogenetic analyses.

228 The alternative whole-genome shotgun sequencing approach applied to 44 taxa produced an

229 average of 8,596,218 raw reads per individual. All new sequence data are available for download

230 at NBCI SRA numbers can be found in Supplementary Table S1. We extracted the same 546

231 exons retained by the exon-capture protocol from each genome using HMMER v3.1b (Wheeler

232 and Eddy 2013). These sequences were combined with the previously assembled exons to build

233 alignments for each exon, including all taxa. The resulting concatenated matrix with 546 exons

234 was 81% complete (on average, only 19% of the loci could not be sequenced for each taxon).

235 But missing data are not evenly distributed among taxa, affecting disproportionally eight species

236 with data coverage below 50%. At the lower end, only 7% and 13% of loci could be sequenced

237 for the two outgroup anguilliform taxa (*Kaupichthys hyporoides* and *Gymnothorax reevesii*,

238 respectively). Data coverage ranged from 20-49% for five Mormyrids (*Petrocephalus balayi,*

239 *Marcusenius sanagaensis, Paramormyrops batesii, Petrocephalus sp1,* and *Stomatorhinus*

240 *fuliginosus*) and for the outgroup *Amia calva*. The African butterflyfish *Pantodon buchholzi*

241 could be sequenced for 56% of all loci. Two *Myomyrus pharaoh* individuals were sequenced

242 separately using both target capture and the shotgun genome approach. The placement of the two

243 *M. pharaoh* tips as sister taxa in the phylogeny (Fig. 2) establishes confidence for the

244 combination of different approaches used to collect data. All alignments are available in

245 Appendix 1 (Supplementary Materials).

246

247 ***Phylogenetic Inference and Divergence Estimation for Osteoglossomorpha.—***

248 Collectively, our results (Fig. 1e) support the hypothesis for family-level relationships of

249 Osteoglossomorpha published by Lavoué and Sullivan (2004), and Betancur-R et al. (2017). The

250 only exceptions were (i) the tree inferred with ASTRAL for subset 6 that placed Pantondidae

251 (instead of Hiodontidae) as the sister group to all osteoglossomorphs, (ii) the trees inferred with

252 both ASTRAL and IQ-TREE for subset 8 and the tree inferred with IQ-TREE for subset 10

253 places Pantondidae as the sister-group of Osteoglossidae, and (iii) the tree inferred with IQ-

254   TREE for subset 3 places Pantondidae as the sister-group to outgroup taxa in Anguilliformes

255   (Supplementary Fig. S1). High proportion of missing data for *Pantodon* and anguilliform taxa in

256   these subsets may account for the discordant results (Supplementary Table S7). The distribution

257   of alternative topologies in MDS tree space is displayed in Supplementary Figure S2, showing

258   non-overlapping positions for IQ-TREE and ASTRAL trees. Trees inferred with IQ-TREE for

259   subset 8 and subset 3 are outliers in MDS space (Supplementary Fig. S2), likely due to the rogue

260   position of Pantondidae and anguilliforms mentioned above.

261   Other issues that should be considered to explain differences in time-tree estimation is

262   sampling (taxa and loci) and methodology used. Our study analyzed the largest data matrix to

263   date, and we assessed the variance or uncertainty of estimated ages by analyzing 10 non-

264   overlapping gene subsets sampled from the complete dataset. Exons used in this study are

265   evolutionarily conserved, avoiding overestimation typically obtained with rapidly evolving

266   molecular markers. In addition, different methods may converge on diverse estimates even when

267   using the same data (Arcila et al. 2017, 2020). Lavoué (2016) used a tip-dating approach

268   (implemented in MrBayes and BEAST) based on multiple fossils but only six molecular

269   markers. Tip-dating approaches using standard Bayesian MCMC sampling have many desirable

270   properties but are computationally intractable for genome-scale alignments and inapplicable for

271   our dataset. The MCMCTree method implemented in this study uses a multivariate uniform

272   distribution approximation to estimate likelihoods of branch lengths which speeds up

273   computation substantially but may be less desirable than a full likelihood implementation. The

274   compromise between data size and choice of method certainly deserves further scrutiny, but our

275   conservative approach suggests that we obtained a robust time-calibration for the divergence of

276   bony-tongue fishes.

277   We found including a fossil calibration based on †*Scleropages sinensis* did not change

278   the overall results significantly (See Supplementary Appendix 2). Results were similar to those

279   reported in main text with most nodes in the time-tree changing by 0-10 Ma, without altering our

280   general conclusions. However, the age for the split of *Scleropages* (SE Asia and Australia)

281   and *Osteoglossum* (South America) changed from 38.2 Ma (95% HPD of 24.9–50.9) to 52 Ma

282   (95% HPD of 48.6–55.6 Ma) as this fossil has direct bearing on this particular branch. This

283   discrepancy affects our original conclusion about a biogeographic hypothesis for osteoglossids,

284   given that the separation between Australia and South America/Antarctica is dated to ~64 Ma

285   (Woodburne and Case 1996; Black et al. 2012) or 43 Ma (Brown et al. 2006), changing our

286   interpretation slightly in favor of vicariance to explain the *Osteoglossum/Scleropages*

287   disjunction. However, we chose not to rerun all our comparative analyses based on this revised

288   time tree (BioGeoBears and SIMMAP) given that the focus of the paper is on mormyrids, and

289   the ages inferred for mormyrids remain largely unaffected. The estimated age of crown

290   mormyrids changed from 52 Ma (HPD 44.6-58.9) to 60.2 Ma (HPD 46.8-83.19) and for Clade

291   C+ from 13.1 Ma (HPD 11-15) to 17.6 Ma (HPD 11.7-37.7). Only the upper bounds of the HPD

292   intervals increased, but the ages of the nodes in the calibrated tree that is used for comparative

293   analyses remained virtually the same.

294

295   ***Taxonomic Findings.***— To our knowledge, this is the first study to publish a sequence of

296   *Gnathonemus echidnorhynchus,* a species that is more closely related to a group of *Marcusenius*

297   species than to *G. petersii* (Fig. 3). Our results also support a novel placement for *Hyperopisus*

298   *bebe* as sister to a clade that groups *Stomatorhinus, Pollimyrus*, *Brevimyrus, Cryptomyrus,*

299   *Boulengeromyrus, Ivindomyrus*, *Marcusenius*, and *Paramormyrops,* in contrast to previous

300   phylogenetic studies that found weak support for *H. bebe* as sister to *Brevimyrus niger* or *B.*

301   *niger* and *Hippopotamyrus pictus*. Also unlike previous phylogenetic hypotheses (Sullivan,

302   Lavoué, and Hopkins 2000; Lavoué et al. 2000; Sullivan, Lavoué, and Hopkins 2002), we find

303   that *B. niger* is the sister group to a clade that contains *Cryptomyrus*, *Boulengeromyrus*,

304   *Ivindomyrus*, and *Paramormyrops*.

305   In agreement with Sullivan, Lavoué, and Hopkins (2000) we find that *Marcusenius* and

306   *Hippopotamyrus* are non-monophyletic, we further show the genus *Gnathonemus* is

307   polyphyletic. The inclusion in our study of type species for many genera can be used to identify

308   taxa in particular need of formal taxonomic revision. The type species of the genus *Marcusenius*

309   is *M. cyprinoides* (Gill 1862), which forms a clade with *M. krameri, M. pongolensis, M.*

310   *altisambesi, M. marcolepidotus, M. senegalensis, M. mento,* and *M. ussheri* (Fig. 3). All other

311   *Marcusenius* require new generic denominations. The type species of *Hippopotamyrus* is *H.*

312   *castor* (Pappenheim 1906), which groups with *H. pictus* and *H. paugi;* other species of the so-

313   called *"Hippopotamyrus ansorgii* complex*"* cluster elsewhere in our phylogeny (Fig. 3). Finally,

314   the type species for the genus *Gnathonemus* is *G. petersii* (Gill 1862) which only groups with *G.*

315   *longibarbis* in our tree (Fig. 3) suggesting that *G. echidnorhynchus* needs taxonomic revision.

316

317   ***Biogeographic Analyses of Mormyridae in Africa.***—Biogeographic hypotheses obtained with

318   different models were overall similar but differed significantly by assigning the ancestral range

319   for all mormyrids (the root node) to either the CB (with models M0-DEC, M0-DEC +*j*, and M1-

320   DEC+*w*+ *j*) or to a much broader range comprising the Nilo-Sudanic, Upper Guinea, Lower

321   Guinea, Congo Basin, and the Zambezi regions (NS+UG+LG+CB+Z) with the preferred model

322   M1-Dec+*w*. (Fig, 4a). All models, however, estimated multiple range reductions from broad

323   ancestral ranges for the most basal nodes of mormyrids to either the Nilo-Sudanic region or to

324   the Congo Basin, and a colonization event of *Paramormyrops* into the Lower Guinea region.

325   Mormyrids present in the East Coast region (Rift Lakes) always originated from relatives in the

326   Congo Basin (six independent colonization events from CB to EC, Fig. 4a). Further Upper

327   Guinea mormyrids originated from Nilo-Sudanic ancestors (seven independent colonization

328   events from NS to UG, Fig. 4a).

329   Independent transitions among CFM states were examined in a biogeographic context.

330   The ancestral blunt-nosed phenotype and the chin-swelling state have a broad distribution

331   occupying multiple basins with no discernable pattern (green and gray symbols, Fig. 4b).

332   However, this is not the case for the tubesnout and tubesnout with Schnauzenorgan CFMs

333   (orange and yellow symbols, Fig. 4b). The estimated geographic setting involving transitions to

334   these two CFMs is consistent across different dispersal matrices and range models

335   (Supplementary Table S9) and involve four origins of tubesnout and three for tubesnouts with

336   Schnauzenorgan. The first transition to tubesnout leads to *Mormyrops caballus* (TS1 in Fig. 4,

337   also see Fig. 2) mapping to the NSUGLGCBZ region (Fig. 4a). The second transition to

338   tubesnout was estimated for the MRCA of *Mormyrops zanclirostris* and *Mormyrops boulengeri*

339   (TS2 in Fig. 4, also see Fig. 2), and the third transition involves *Mormyrus caballus* (TS3 in Fig.

340   4, also see Fig. 2), both mapping to the CB (Fig. 4a). The fourth transition into tubesnouts was

341   inferred for the MCRA of *Mormyrus proboscirostris* and *Mormyrus rume* (TS4 in Fig. 4, also

342   see Fig. 2), mapping to the Lower Guinea, Congo Basin, and Zambezi (LGCBZ). Finally, the

343   three transitions into tubesnout with Schnauzenorgan for *Genyomyrus donnyi*

344   (TS+S1) *Gnathonemus echidnorhynchus* (TS+S2), and the MRCA of *Campylomormyrus*

345   (TS+S3, Fig. 4) were inferred to have occurred in the CB (also see Fig. 2). A CB ancestral rang

346   was also hypothesized for the Schnauzenorgan of *Gnathonemus petersii* and *Gnathonemus*

347   *longibarbis*.

348

349

350   SUPPLEMENTARY FIGURES

351

352
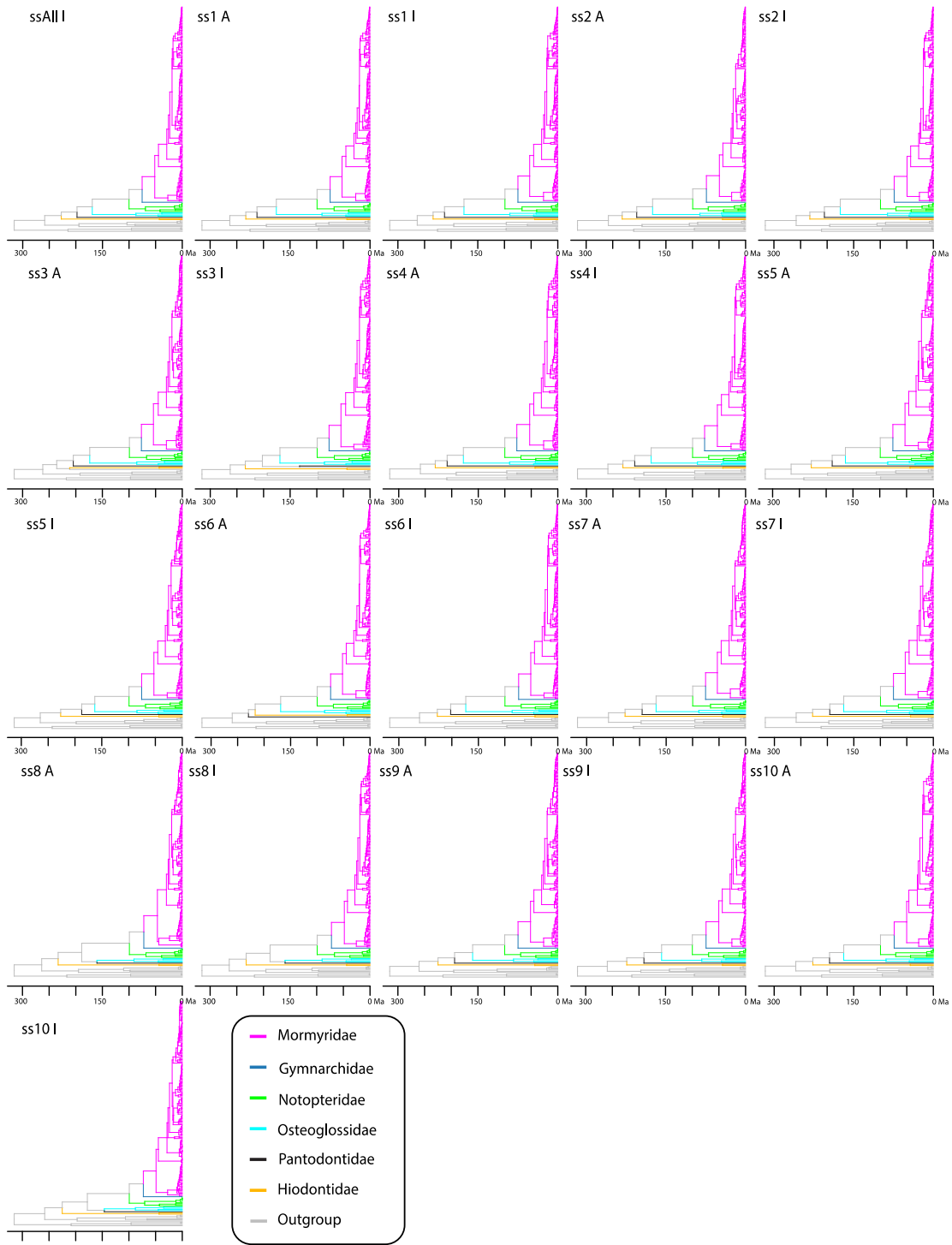
Figure S1: Time trees for Osteoglossomorpha for each of the 21 topologies obtained by analysis of subsets (ss1 – ss10) or the complete data matrix (ssAll). Topologies inferred with IQ-TREE on concatenated data and with ASTRAL on gene trees are labeled I and A, respectively.

356

357
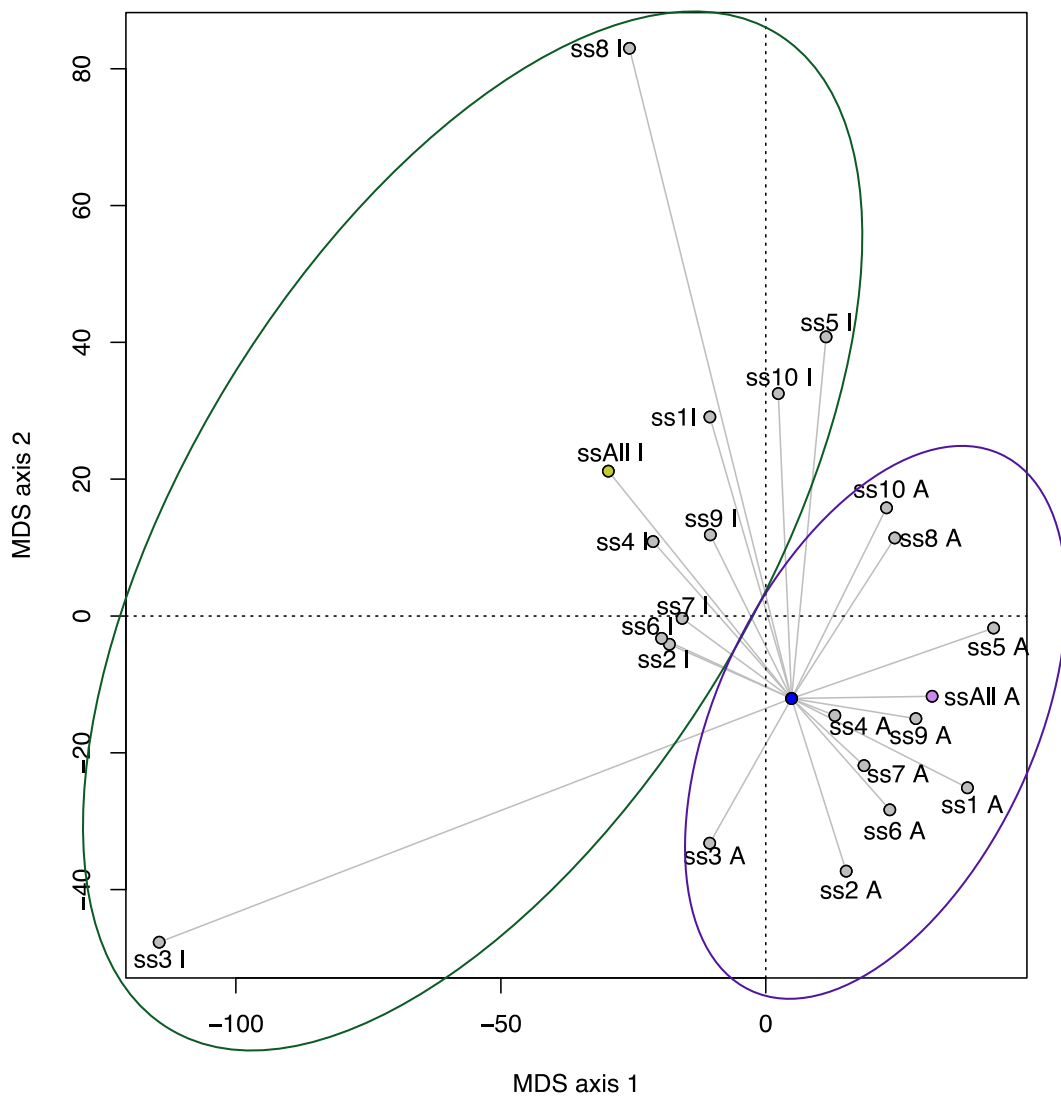
Figure S2: Multi-dimensional space plot for 22 tree topologies estimated in this study from analyses of 11 data subsets (ss1-ss10) and the complete data matrix (ssAll I light green and ssAll A light purple). Dark Green circle denotes the subsets that were concatenated and analyzed with IQ-Tree (labels ending with "I"). The dark purple circle contains trees inferred with ASTRAL (labels ending with "A"). The centroid tree is indicated by the blue dot.

364

365

366

367

368

369

370

371

372

373

374

375

376

377
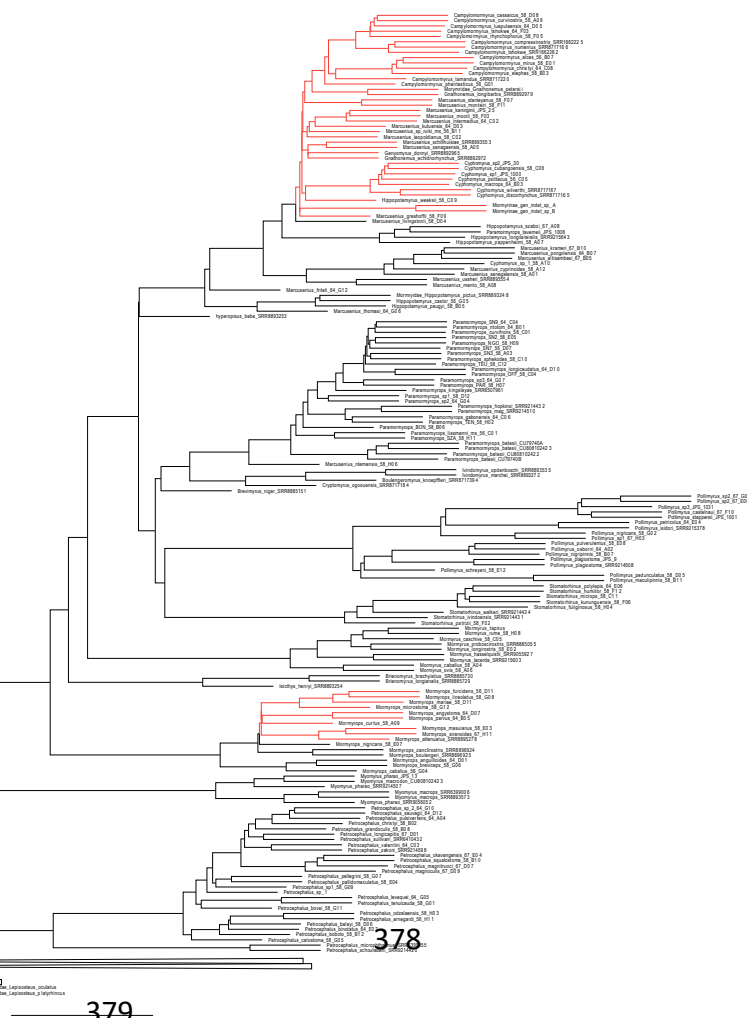
380 **Figure S3:** Tree inferred with ASTRAL using the whole dataset. Tree is collapsed to family

381 level to highlight in red the polytomies present within Mormyridae.

382

383

384

385

386
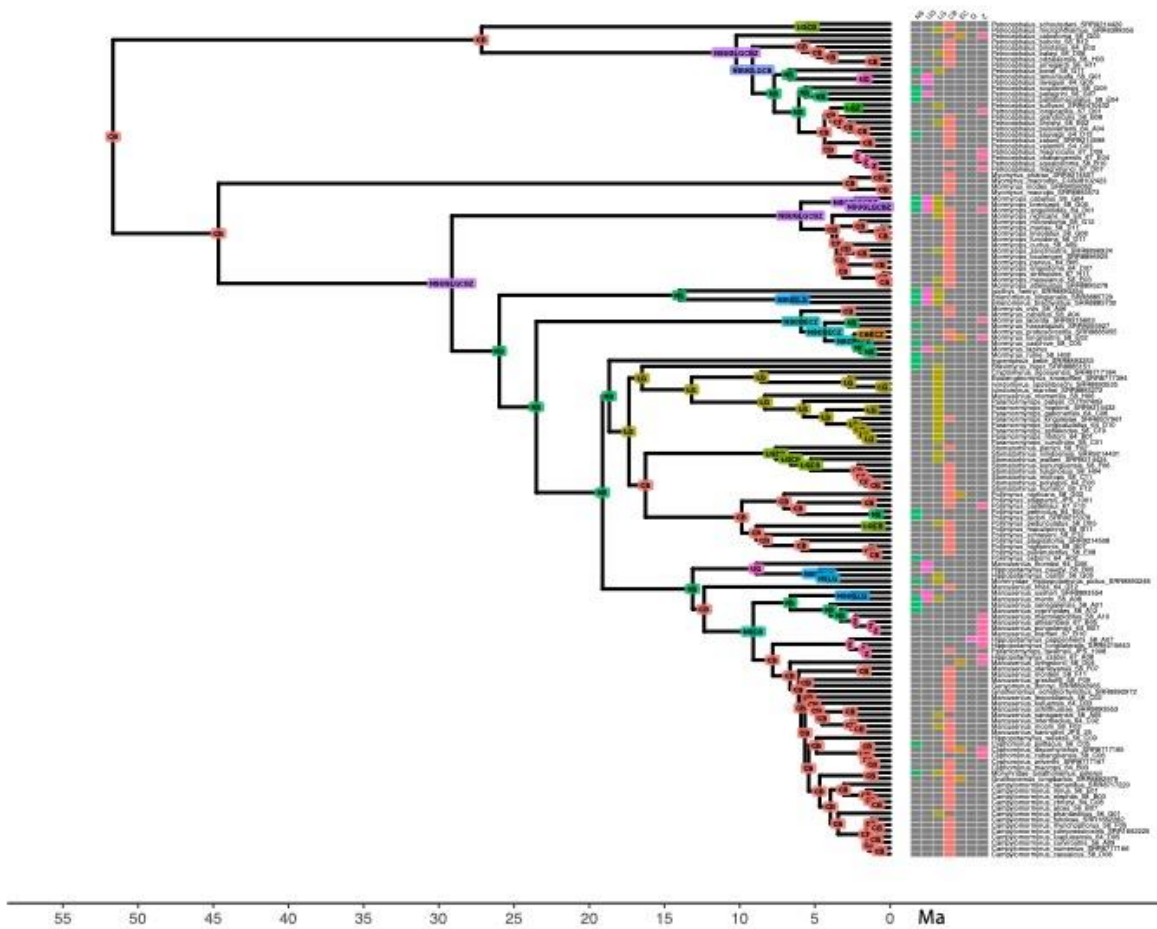
Figure S4: Ancestral Range Estimation for Mormyridae using the best fitting model overall,

DEC+*w*+*j* for M1 dispersal matrix. Boxes at nodes represent the geographic range.

389
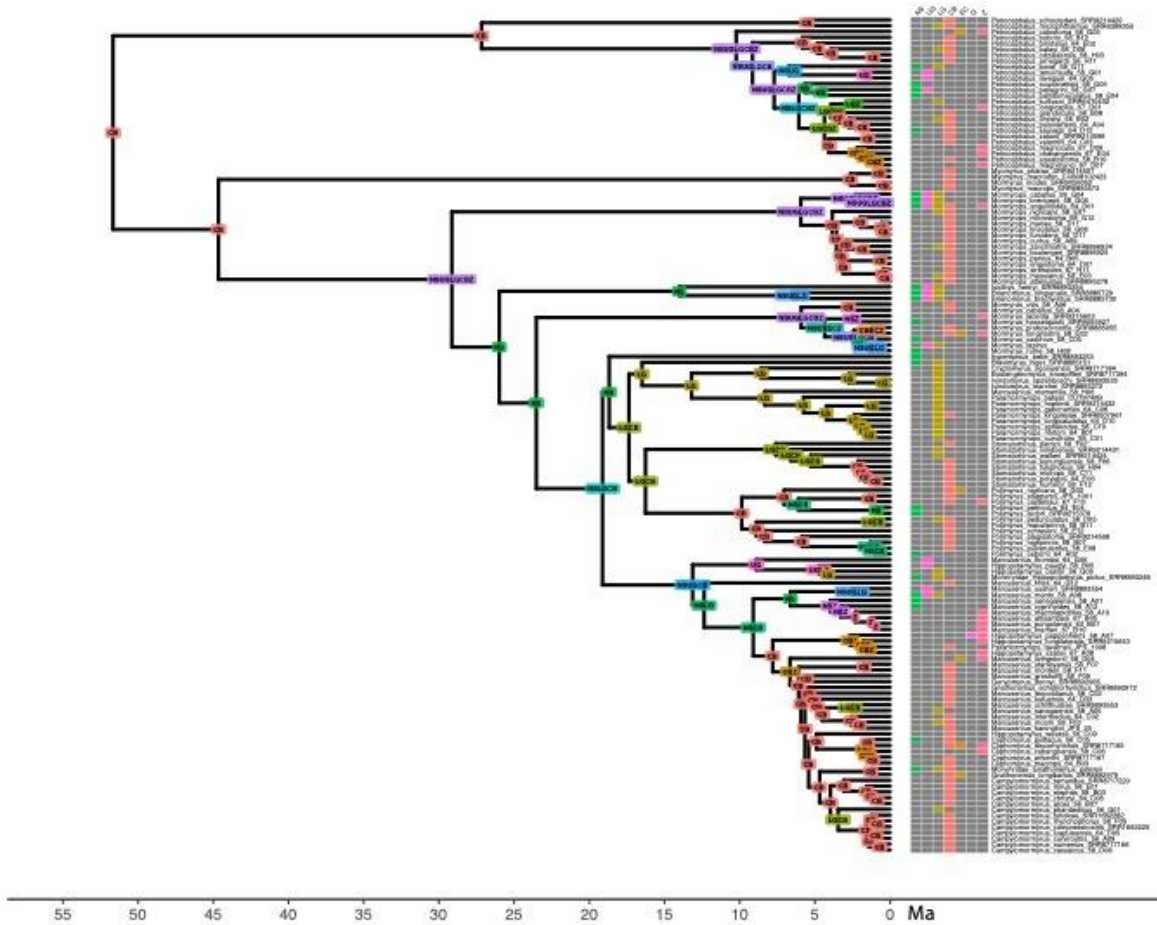
390

391 **Figure S5**: Ancestral Range Estimation for Mormyridae using the best fitting model excluding

392 +*j* parameter (DEC) for the M0 dispersal matrix. Boxes at nodes represent the geographic range.

393

394

395

396

397

398

399

401   **Table S1**: List of taxa examined in this study.

| Species Name	Institution	Voucher	SRA Number	Sequencing Method
Arapaima gigas	Publicly Available	Publicly Available	PRJEB22808	Short Read Genome
Arapiama cf. gigas	Stewart	07-A14	PRJNA699339	Target Capture
Arapiama cf. gigas	Stewart	07-D15	PRJNA699339	Target Capture
Arapiama gigas	USNM	440586	PRJNA699339	Target Capture
Boulengeromyrus knoepffleri	CUMV	81643 tag 2254	PRJNA699339	Target Capture
Brevimyrus niger	CUMV	94596	SRR8885151	Short Read Genome
Brienomyrus brachyistius	CUMV	89979	SRR8885730	Short Read Genome
Brienomyrus longianalis	AMNH	257030	SRR8885729	Short Read Genome
Campylomormyrus alces	CUMV	96469	PRJNA699339	Target Capture
Campylomormyrus cassaicus	AMNH	268580	PRJNA699339	Target Capture
Campylomormyrus cf. tshokwe 1	AMNH	247394	PRJNA699339	Target Capture
Campylomormyrus cf. tshokwe 2	Publicly Available	Publicly Available	SRX767436	Short Read Genome
Campylomormyrus christyi	AMNH	246264	PRJNA699339	Target Capture
Campylomormyrus compressirostris	Publicly Available	Publicly Available	SRX767403	Short Read Genome
Campylomormyrus curvirostris	CUMV	97049	PRJNA699339	Target Capture
Campylomormyrus elephas	AMNH	236803	PRJNA699339	Target Capture
Campylomormyrus luapulaensis	CUMV	91224	PRJNA699339	Target Capture
Campylomormyrus mirus	CUMV	97045	PRJNA699339	Target Capture
Campylomormyrus numenius	CUMV	97364	SRR8717166	Short Read Genome
Campylomormyrus phantasticus	CUMV	89956	PRJNA699339	Target Capture
Campylomormyrus rhynchophorus	CUMV	97365	PRJNA699339	Target Capture
Campylomormyrus tamandua	CUMV	87879	SRR8717220	Short Read Genome
Chitala blanci	FLMNH	172896	PRJNA699339	Target Capture
Chitala borneensis	FLMNH	161800	PRJNA699339	Target Capture
Chitala chitala	SAIAB	186052	SRR9214421	Short Read Genome
Chitala ornata	Hughes et al 2018	Hughes et al 2018	Hughes et al 2018	Transcriptome

Cryptomyrus ogoouensis	CUMV	98155	PRJNA699339	Target Capture
Cyphomyrus cubangoensis	AMNH	268989	PRJNA699339	Target Capture
Cyphomyrus discorhynchus	CUMV	82809	SRR8717165	Short Read Genome
Cyphomyrus macrops	AMNH	242358	PRJNA699339	Target Capture
Cyphomyrus psittacus	CUMV	96391	PRJNA699339	Target Capture
Cyphomyrus sp. 1	Sullivan	JPS_1000	PRJNA699339	Target Capture
Cyphomyrus sp. 2	Sullivan	JPS_30	PRJNA699339	Target Capture
Cyphomyrus wilverthi	AMNH	253525	SRR8717167	Short Read Genome
Genyomyrus donnyi	CUMV	96735	SRR8892965	Short Read Genome
Gnathonemus echidnorhynchus	CUMV	96186	SRR8892972	Short Read Genome
Gnathonemus longibarbis	CUMV	90412	SRR8892979	Short Read Genome
Gnathonemus petersii	Hughes et al 2018	Hughes et al 2018	Hughes et al 2018	Transcriptome
Gymnarchus niloticus	CUMV	94655	SRX3491732	Short Read Genome
Heterotis niloticus	CUMV	94695	PRJNA699339	Target Capture
Hiodon alosoides	KU	39507	SRR9215630	Short Read Genome
Hiodon tergisus	BMUM	PB00-22	SRR9214422	Short Read Genome
Hippopotamyrus castor	CUMV	89955	PRJNA699339	Target Capture
Hippopotamyrus longilateralis	SAIAB	78793	SRR9215643	Short Read Genome
Hippopotamyrus pappenheimi	AMNH	247102	PRJNA699339	Target Capture
Hippopotamyrus paugyi	CUMV	97660	PRJNA699339	Target Capture
Hippopotamyrus pictus	CUMV	94598	SRR8893248	Short Read Genome
Hippopotamyrus szaboi	SAIAB	204161	PRJNA699339	Target Capture
Hippopotamyrus weeksii	CUMV	87741	PRJNA699339	Target Capture
hyperopisus bebe	CUMV	91467	SRR8893253	Short Read Genome
Isicthys henryi	CUMV	84650 -2051	SRR8893254	Short Read Genome
Ivindomyrus marchei	CUMV	83105	SRR8893272	Short Read Genome
Ivindomyrus opdenboschi	CUMV	83107	SRR8893535	Short Read Genome
Marcusenius altisambesi	SAIAB	85238	PRJNA699339	Target Capture
Marcusenius cyprinoides	CUMV	94595	PRJNA699339	Target Capture
Marcusenius friteli	CUMV	87842	PRJNA699339	Target Capture
Marcusenius greshoffii	CUMV	96731	PRJNA699339	Target Capture
Marcusenius intermedius	AMNH	252800	PRJNA699339	Target Capture
Marcusenius kaninginii	Sullivan	JPS_25	PRJNA699339	Target Capture

Marcusenius krameri	SAIAB	188290	PRJNA699339	Target Capture
Marcusenius kutuensis	AMNH	241911	PRJNA699339	Target Capture
Marcusenius leopoldianus	CUMV	88154	PRJNA699339	Target Capture
Marcusenius livingstonii	CUMV	93897	PRJNA699339	Target Capture
Marcusenius macrolepidotus	CUMV	96770	PRJNA699339	Target Capture
Marcusenius mento	CUMV	97713	PRJNA699339	Target Capture
Marcusenius monteiri	CUMV	96194	PRJNA699339	Target Capture
Marcusenius moorii	CUMV	87868	PRJNA699339	Target Capture
Marcusenius ntemensis	CUMV	92264	PRJNA699339	Target Capture
Marcusenius pongolensis	AMNH	258953	PRJNA699339	Target Capture
Marcusenius sanagaensis	CUMV	93237	PRJNA699339	Target Capture
Marcusenius schilthuisiae	CUMV	87790	PRJNA699339	Target Capture
Marcusenius senegalensis	CUMV	97708	PRJNA699339	Target Capture
Marcusenius sp. 'ruiki' ms	CUMV	96192	PRJNA699339	Target Capture
Marcusenius stanleyanus	CUMV	94097	PRJNA699339	Target Capture
Marcusenius thomasi	AMNH	257037	PRJNA699339	Target Capture
Marcusenius ussheri	CUMV	97730	SRR8893554	Short Read Genome
Mormyrinae gen. indet. sp. A	CUMV	91920	PRJNA699339	Target Capture
Mormyrinae gen. indet. sp. B	CUMV	91923	PRJNA699339	Target Capture
Mormyrops anguilloides	CUMV	89968	PRJNA699339	Target Capture
Mormyrops attenuatus	CUMV	88155	SRR8895278	Short Read Genome
Mormyrops boulengeri	CUMV	87730	SRR8896925	Short Read Genome
Mormyrops breviceps	CUMV	93231	PRJNA699339	Target Capture
Mormyrops caballus	CUMV	89970	PRJNA699339	Target Capture
Mormyrops curtus	AMNH	256207	PRJNA699339	Target Capture
Mormyrops engystoma	AMNH	268392	PRJNA699339	Target Capture
Mormyrops furcidens	CUMV	97529	PRJNA699339	Target Capture
Mormyrops lineolatus	CUMV	88160	PRJNA699339	Target Capture
Mormyrops mariae	AMNH	254545	PRJNA699339	Target Capture
Mormyrops masuianus	CUMV	88156	PRJNA699339	Target Capture
Mormyrops microstoma	AMNH	253568	PRJNA699339	Target Capture
Mormyrops nigricans	CUMV	96831	PRJNA699339	Target Capture
Mormyrops parvus	AMNH	250367	PRJNA699339	Target Capture
Mormyrops sirenoides	AMNH	251067	PRJNA699339	Target Capture
Mormyrops zanclirostris	CUMV	96834	SRR8896924	Short Read Genome
Mormyrus caballus	CUMV	88403	PRJNA699339	Target Capture
Mormyrus caschive	CUMV	94651	PRJNA699339	Target Capture
Mormyrus hasselquistii	CUMV	94650	SRR9055927	Short Read Genome
Mormyrus lacerda	SAIAB	87199	SRR9215603	Short Read Genome
Mormyrus longirostris	CUMV	93890- JPF 1018	PRJNA699339	Target Capture

Mormyrus ovis	CUMV	96183	PRJNA699339	Target Capture
Mormyrus proboscirostris	CUMV	96245	SRR8885055	Short Read Genome
Mormyrus rume	CUMV	97706	PRJNA699339	Target Capture
Mormyrus tapirus	Hughes et al 2018	Hughes et al 2018	Hughes et al 2018	Transcriptome
Myomyrus macrodon	CUMV	808102423	PRJNA699339	Target Capture
Myomyrus macrops	AMNH	231025	SRR6399006	Short Read Genome
Myomyrus macrops			SRR8893573	Short Read Genome
Myomyrus pharao	CUMV	96474	SRR9214507	Short Read Genome
Myomyrus pharao	Sullivan	JPS_13	PRJNA699339	Target Capture
Myomyrus sp. 2	AMNH	263510	SRR9056052	Short Read Genome
Notopterus notopterus	AUMNH	AUFT3812	PRJNA699339	Target Capture
Osteoglossum bicirrhosum	Hughes et al 2018	Hughes et al 2018	Hughes et al 2018	Transcriptome
Pantodon buchholzi	Hughes et al 2018	Hughes et al 2018	Hughes et al 2018	Target Capture
Papyrocranus afer	Hughes et al 2018	Hughes et al 2018	Hughes et al 2018	Target Capture
Papyrocranus congoensis	AMNH	244153	PRJNA699339	Target Capture
Paramormyrops batesii	CUMV	CU79740A	PRJNA699339	Target Capture
Paramormyrops batesii	CUMV	CU808102422	PRJNA699339	Target Capture
Paramormyrops batesii	CUMV	CU808102423	PRJNA699339	Target Capture
Paramormyrops curvifrons	CUMV	89359-5609	PRJNA699339	Target Capture
Paramormyrops gabonensis	CUMV	94162 - 5598	PRJNA699339	Target Capture
Paramormyrops hopkinsi	CUMV	89281 - 5497	SRR9214432	Short Read Genome
Paramormyrops kingsleyae	Hughes et al 2018	Hughes et al 2018	Hughes et al 2018	Transcriptome
Paramormyrops lissmanni ms	CUMV	81090 tag 3365	PRJNA699339	Target Capture
Paramormyrops longicaudatus	CUMV	96846	PRJNA699339	Target Capture
Paramormyrops MAG	CUMV	98100	PRJNA699339	Target Capture
Paramormyrops ntotom	CUMV	83075	PRJNA699339	Target Capture
Paramormyrops sp. 1	AMNH	268595	PRJNA699339	Target Capture
Paramormyrops sp. 2	AMNH	236173	PRJNA699339	Target Capture
Paramormyrops sp. 4	AMNH	231490	PRJNA699339	Target Capture
Paramormyrops sp. BON	CUMV	80307 -2988	PRJNA699339	Target Capture
Paramormyrops sp. NGO	CUMV	80317 -3002	PRJNA699339	Target Capture
Paramormyrops sp. OFF	CUMV	83111-4744	PRJNA699339	Target Capture
Paramormyrops sp. PAR	CUMV	80934- 3458	PRJNA699339	Target Capture
Paramormyrops sp. SN2	CUMV	80299 -2960	PRJNA699339	Target Capture
Paramormyrops sp. SN3	CUMV	80356 - 3027	PRJNA699339	Target Capture

Paramormyrops sp. SN7	CUMV	80496 tag 3666	PRJNA699339	Target Capture
Paramormyrops sp. SN9	CUMV	83113 tag 4928	PRJNA699339	Target Capture
Paramormyrops sphekodes	CUMV	98177	PRJNA699339	Target Capture
Paramormyrops SZA	CUMV	75390 - 1321	PRJNA699339	Target Capture
Paramormyrops taverneii	Sullivan	JPS_1008	PRJNA699339	Target Capture
Paramormyrops TEN	CUMV	89361 -5642	PRJNA699339	Target Capture
Paramormyrops TEU	CUMV	98126	PRJNA699339	Target Capture
Petrocephalus arnegardi	CUMV	88027	PRJNA699339	Target Capture
Petrocephalus balayi	CUMV	83327 - 4346	PRJNA699339	Target Capture
Petrocephalus binotatus	AMNH	246324	PRJNA699339	Target Capture
Petrocephalus boboto	CUMV	96774	PRJNA699339	Target Capture
Petrocephalus bovei	CUMV	94594	PRJNA699339	Target Capture
Petrocephalus catostoma	CUMV	93893	PRJNA699339	Target Capture
Petrocephalus christyi	CUMV	97513	PRJNA699339	Target Capture
Petrocephalus grandoculis	CUMV	97475	PRJNA699339	Target Capture
Petrocephalus levequei	AMNH	257032	PRJNA699339	Target Capture
Petrocephalus longicapitis	SAIAB	202283	PRJNA699339	Target Capture
Petrocephalus magnitrunci	SAIAB	202796	PRJNA699339	Target Capture
Petrocephalus magnoculis	SAIAB	78788	PRJNA699339	Target Capture
Petrocephalus microphthalmus	CUMV	97508	SRX3492530	Short Read Genome
Petrocephalus odzalaensis	CUMV	88054	PRJNA699339	Target Capture
Petrocephalus okavangensis	SAIAB	202789	PRJNA699339	Target Capture
Petrocephalus pallidomaculatus	AMNH	256969	PRJNA699339	Target Capture
Petrocephalus pellegrini	CUMV	97724	PRJNA699339	Target Capture
Petrocephalus pulsivertens	AMNH	260685	PRJNA699339	Target Capture
Petrocephalus sauvagii	CUMV	96777	PRJNA699339	Target Capture
Petrocephalus schoutedeni	CUMV	97510	SRR9214420	Short Read Genome
Petrocephalus soudanensis	AMNH	256985	PRJNA699339	Target Capture
Petrocephalus sp. 1	CUMV	91327	SRX3828586	Short Read Genome
Petrocephalus sp. 2	AMNH	270503	PRJNA699339	Target Capture
Petrocephalus squalostoma	CUMV	91142	PRJNA699339	Target Capture
Petrocephalus sullivani	CUMV	79700	SRX3503552	Short Read Genome
Petrocephalus tenuicauda	AMNH	254119	PRJNA699339	Target Capture
Petrocephalus valentini	AMNH	255279	PRJNA699339	Target Capture
Petrocephalus zakoni	CUMV	87787	SRR9214598	Short Read Genome
Pollimyrus castelnaui	SAIAB	68502	PRJNA699339	Target Capture
Pollimyrus isidori	CUMV	97714	SRR9215378	Short Read Genome
Pollimyrus maculipinnis	AMNH	268405	PRJNA699339	Target Capture
Pollimyrus nigricans	CUMV	97966	PRJNA699339	Target Capture
Pollimyrus nigripinnis	CUMV	96794	PRJNA699339	Target Capture

Pollimyrus osborni	AMNH	268624	PRJNA699339	Target Capture
Pollimyrus pedunculatus	AMNH	260774	PRJNA699339	Target Capture
Pollimyrus petricolus	AMNH	254098	PRJNA699339	Target Capture
Pollimyrus plagiostoma	CUMV	96188	SRR9214508	Short Read Genome
Pollimyrus plagiostoma	Sullivan	JPS_9	PRJNA699339	Target Capture
Pollimyrus pulverulentus	AMNH	268626	PRJNA699339	Target Capture
Pollimyrus schreyeni	AMNH	241897	PRJNA699339	Target Capture
Pollimyrus sp. 1	SAIAB	73892 - N181	PRJNA699339	Target Capture
Pollimyrus sp. 2	SAIAB	67706 - 197	PRJNA699339	Target Capture
Pollimyrus sp. 2	SAIAB	67639 - 217	PRJNA699339	Target Capture
Pollimyrus sp. 3	Sullivan	JPS_1031	PRJNA699339	Target Capture
Pollimyrus stappersii	Sullivan	JPS_1001	PRJNA699339	Target Capture
Scleropages formosus	Hughes et al 2018	Hughes et al 2018	Hughes et al 2018	Transcriptome
Stomatorhinus fuliginosus	AMNH	242247	PRJNA699339	Target Capture
Stomatorhinus humilior	AMNH	268408	PRJNA699339	Target Capture
Stomatorhinus ivindoensis	CUMV	92286	SRR9214431	Short Read Genome
Stomatorhinus kununguensis	AMNH	268413	PRJNA699339	Target Capture
Stomatorhinus microps	AMNH	255421	PRJNA699339	Target Capture
Stomatorhinus patrizii	CUMV	87991	PRJNA699339	Target Capture
Stomatorhinus polylepis	AMNH	268416	PRJNA699339	Target Capture
Stomatorhinus walkeri	CUMV	95160	SRR9214424	Short Read Genome
Xenomystus nigri	CUMV	87791	PRJNA699339	Target Capture

402

403

404

405

406

407

408

409

410

411

412

413   **Table S2**: Ages for Ostelgossomorpha clades inferred by previous studies (millions of years ago)

Study	Osteoglossomorpha	95% HPD	Osteoglossiformes	95% HPD	Mormyroidea	95% HPD
Peterson et al., 2021	227.4	248.8-207	197.7	221.6-174.4	75.3	82.9-67.5
Betancur et al., 2017	227	-	160	-	50	-
Broughton et al., 2013	230	260-197	189.2	230.2-148.5	80	150-50
Lavoué 2016	175	190-148	140	176-125	66	90-40
Hughes et al., 2018	-	-	190	240-150	-	-
Capobianco and Friedman 2018	182.2		-	-	-	-

414

415

416

417

418

419

420

421

422

423

424

425

426

427

428

429

430

431   **Table S3**: Priors used for estimation of divergence times in MCMCTree.

MCRA	Fossil and absolute Age	Distribution	Calibration Type	Parameters
Holesti and Osteoglossomorpha Node A in Figure 1E	Secondary calibration	Uniform	Soft upper bound and Soft lower bounds	B(300,328,0.025,0.025)
***Atractosteus* and *Lepisosteus* Node B in Figure 1E**	*†Atractosteus falipoui* Africa, Upper Cretaceous Cenomanian (100.5-93.9 Ma.)	Uniform	Hard upper bound and soft lower bound	B(93.9,145,1e-300,0.05)
***Megalops* and *Anguilla* Node C in Figure 1E**	Secondary calibration	Uniform	Soft upper bound and Soft lower bounds	B(180,215,0.025,0.025)
Elopomorpha and Osteoglossomorpha	Secondary calibration	Uniform	Soft upper bound and Soft lower bounds	B(249,284,0.025,0.025)
Hiodon alosoides* and *Hiodon tergisus	†*Eohiodon woodruffi* Paleogene, Eocene, Lutetian (41.3-47.8 Ma.)	Uniform	Hard upper bound and soft lower bound	B(41.3,47.8,1e-300,0.05)
Heterotis niloticus* and *Arapiama gigas	†Sinoglossus lushanensis East Asia (freshwater), Paleogene, Eocene, Lutetian (41.3-47.8 Ma.)	Uniform	Hard upper bound and soft lower bound	B(41.3,47.8,1e-300,0.05)
Notopteridae* and *Gymnarchus niloticus	†Palaeonotopterus greenwoodi African Freshwater; Upper Cretaceous, C enomanian (93.9 - 100.5)	Uniform	Hard upper bound and soft lower bound	B(93.9, 100.5,1e-300,0.05)

432

433

434

435

29

436   **Table S4**: AICc scores for three different discreet morphology models tested for each 21

437   topologies obtained by analysis of subsets (ss1 – ss10) or the complete data matrix (ssAll).

438   Topologies inferred with IQ-TREE on concatenated data and with ASTRAL on gene trees are

439   labeled I and A, respectively.

Model Subset	ER	SYM	ARD
ss1 A	137	138.3	155.3
ss1 I	150.4	149.9	167
ss2 A	146.4	146.8	164.2
ss2 I	152.3	151.1	168
ss3 A	149.5	151.1	167.7
ss3 I	156.8	155.1	167.9
ss4 A	152.2	153.6	168.7
ss4 I	151.8	151.7	167.4
ss5 A	142	142.8	158.6
ss5 I	149.6	149.5	163.9
ss6 A	149.6	149.4	165.6
ss6 I	148.5	149.9	165.8
ss7 A	152.6	152.9	168.6
ss7 I	152.3	154.4	170.3
ss8 A	146.1	146.1	163
ss8 I	164.7	161.2	175.8
ss9 A	149.1	149.3	165.7
ss9 I	149.9	149.9	166.4
ss10 A	151.2	151.2	167.6
ss10 I	151.2	151.2	167.6
ssAll I	150.3	150	166.5

440

441

442

443

444

445

446

447 **Table S5**: Divergence time estimates in million years for select Osteoglossomorpha clades (clade

448 names or MRCA indicated) based on the trees obtained from analyses of 11 data subsets (SS1-

449 SS10) and the complete data matrix (SSAll). Topologies inferred with IQ-TREE on concatenated

450 data and with ASTRAL on gene trees are denoted by I and A, respectively. Number of

451 generations ran in MCMCTree indicated in column N (in millions).

	ssAll I	ss1 A	ss1 I	ss2 A	ss2 I	ss3 A	ss3 I	ss4 A	ss4 I	ss5 A	ss5 I	ss6 A	ss6 I	ss7 A	ss7 I	ss8 A	ss8 I	ss9 A	ss9 I	ss10 A	ss10 I
N	7.5	4.5	4.5	4.5	4.5	4.5	4.5	4.5	4.5	4.5	4.5	4.5	4.5	4.5	4.5	4.5	4.5	4.5	4.5	4.5	4.5
Osteoglossmorpha	227.4	233	233.8	232.2	232.5	235.8	234.2	230.9	231.1	227.9	226.5	229.7	227.5	227.5	227.7	233.2	232.3	224.8	222.9	226.9	225.8
Osteoglossiformes	197.7	211.9	212.5	204.8	205.2	204.7	202.2	208.5	208.9	188.8	187.4	216.8	202.1	195.1	195.3	160.2	159.3	193.7	190.7	195.6	146.6
Osteoglossidae	87.2	90	89.9	86	86.3	85.5	85.7	90.7	90.7	85.2	84.5	85.7	86.2	88.2	88.2	90.7	89.9	83.1	82.2	89.1	87.9
Scleropages /Osteoglossum	38.3	40.7	40.5	43.6	43.7	33.3	33.5	42.3	42.2	34	34.2	35.7	35.5	36.5	36.4	36.1	35.1	37.4	37	35	34.7
Arapiama /Heterotis	45.4	45.3	45.2	45.6	45.6	45.1	45.1	45.4	45.4	44.9	45	45.2	45.3	45.2	45.1	44.8	44.9	45.1	45.2	45.3	45.2
Notopteridae	69.3	67.4	67.1	70.3	70.3	67	66.9	69.5	69.4	68.1	68.4	69.2	69.2	66.2	66	68	66.7	69.5	69.5	70.9	70.6
Mormyridae	51.6	52.5	52.6	49.3	49.5	54	54.6	53	53.2	53	52.8	51.9	51.1	53.2	52.9	46.7	48.2	51.2	50.1	50.3	49.2
Clade C+	13.1	13.6	14.3	13.1	13.3	13	13.5	14.2	14.3	15.5	6.3	13.5	13	13.5	13.2	13.7	14.1	13.7	12.6	14.1	12.4

452

453

454

455

456

457

458

459

460

461

462

463

464

465

466 **Table S6**: Distribution of Mormyrids used in the biogeographic analysis. Regions included (and

467 abbreviations) are: Upper Guinea (UG), Lower Guinea (LG), Nilo-Sudanic (NS), Zambezi (Z),

468 East Coast (EC), Congo Basin (CB), and Quanza (Q). Presence (1) or absence (0) in each area is

469 indicated for all species.

Species	1. NS	2. UG	3. LG	4. CB	5. Q	6. Z	7. EC
Boulengeromyrus knoepffleri	0	0	1	0	0	0	0
Brevimyrus niger	1	0	1	0	0	0	0
Brienomyrus brachyistius	1	1	1	0	0	0	0
Brienomyrus longianalis	1	1	1	0	0	0	0
Campylomormyrus alces	0	0	0	1	0	0	0
Campylomormyrus cassaicus	0	0	0	1	0	0	0
Campylomormyrus christyi	0	0	0	1	0	0	0
Campylomormyrus compressirostris	0	0	0	1	0	0	0
Campylomormyrus curvirostris	0	0	0	1	0	0	0
Campylomormyrus elephas	0	0	0	1	0	0	0
Campylomormyrus luapulaensis	0	0	0	1	0	0	0
Campylomormyrus mirus	0	0	0	1	0	0	0
Campylomormyrus numenius	0	0	0	1	0	0	0
Campylomormyrus phantasticus	0	0	1	0	0	0	0
Campylomormyrus rhynchophorus	0	0	0	1	0	0	0
Campylomormyrus tamandua	0	0	0	1	0	0	0
Campylomormyrus tshokwe	0	0	0	1	0	0	0
Cryptomyrus ogoouensis	0	0	1	0	0	0	0
Cyphomyrus cubangoensis	0	0	0	0	0	1	0
Cyphomyrus discorhynchus	0	0	0	1	0	1	1
Cyphomyrus macrops	0	0	0	1	0	0	0
Cyphomyrus psittacus	1	0	0	1	0	0	0
Cyphomyrus wilverthi	0	0	0	1	0	0	0
Genyomyrus donnyi	0	0	0	1	0	0	0
Gnathonemus echidnorhynchus	0	0	0	1	0	0	0
Gnathonemus longibarbis	0	0	0	1	0	0	1
Gnathonemus petersii	1	0	1	1	0	0	0
Hippopotamyrus castor	0	0	1	0	0	0	0
Hippopotamyrus longilateralis	0	0	0	0	0	1	0
Hippopotamyrus pappenheimi	0	0	0	0	1	1	0
Hippopotamyrus paugyi	0	1	0	0	0	0	0
Hippopotamyrus pictus	1	0	1	0	0	0	0
Hippopotamyrus szaboi	0	0	0	0	0	1	0
Hippopotamyrus weeksii	0	0	0	1	0	0	0
Hyperopisus bebe	1	0	0	0	0	0	0
Isicthys henryi	1	1	1	0	0	0	0
Ivindomyrus marchei	0	0	1	0	0	0	0
Ivindomyrus opdenboschi	0	0	1	0	0	0	0
Marcusenius altisambesi	0	0	0	0	0	1	0

Marcusenius cyprinoides	1	0	0	0	0	0	0
Marcusenius friteli	0	0	0	1	0	0	0
Marcusenius greshoffii	0	0	0	1	0	0	0
Marcusenius intermedius	0	0	0	1	0	0	0
Marcusenius kaninginii	0	0	0	1	0	0	0
Marcusenius krameri	0	0	0	0	0	1	0
Marcusenius kutuensis	0	0	0	1	0	0	0
Marcusenius leopoldianus	0	0	0	1	0	0	0
Marcusenius livingstonii	0	0	0	0	0	1	1
Marcusenius macrolepidotus	0	0	0	0	0	1	0
Marcusenius mento	1	1	1	0	0	0	0
Marcusenius monteiri	0	0	0	1	0	0	0
Marcusenius moorii	0	0	1	1	0	0	0
Marcusenius ntemensis	0	0	1	0	0	0	0
Marcusenius pongolensis	0	0	0	0	0	1	0
Marcusenius sanagaensis	0	0	1	0	0	0	0
Marcusenius schilthuisiae	0	0	0	1	0	0	0
Marcusenius senegalensis	1	0	0	0	0	0	0
Marcusenius stanleyanus	0	0	0	1	0	0	0
Marcusenius thomasi	0	1	0	0	0	0	0
Marcusenius ussheri	0	1	0	0	0	0	0
Mormyrops anguilloides	1	1	1	1	0	1	0
Mormyrops attenuatus	0	0	0	1	0	0	0
Mormyrops boulengeri	0	0	0	1	0	0	0
Mormyrops breviceps	1	1	1	0	0	0	0
Mormyrops caballus	1	1	1	0	0	0	0
Mormyrops curtus	0	0	0	1	0	0	0
Mormyrops engystoma	0	0	0	1	0	0	0
Mormyrops furcidens	0	0	0	1	0	0	0
Mormyrops lineolatus	0	0	0	1	0	0	0
Mormyrops mariae	0	0	0	1	0	0	0
Mormyrops masuianus	0	0	1	1	0	0	0
Mormyrops microstoma	0	0	0	1	0	0	0
Mormyrops nigricans	0	0	1	1	0	0	0
Mormyrops parvus	0	0	0	1	0	0	0
Mormyrops sirenoides	0	0	0	1	0	0	0
Mormyrops zanclirostris	0	0	1	1	0	0	0
Mormyrus caballus	0	0	0	1	0	0	0
Mormyrus caschive	1	0	0	0	0	0	0
Mormyrus hasselquistii	1	0	0	0	0	0	0
Mormyrus iriodes	0	0	0	1	0	0	0
Mormyrus lacerda	0	0	0	0	0	1	0
Mormyrus longirostris	0	0	0	1	0	1	1
Mormyrus ovis	0	0	0	1	0	0	0
Mormyrus proboscirostris	0	0	0	1	0	0	0
Mormyrus rume	1	0	0	0	0	0	0
Mormyrus tapirus	0	1	1	0	0	0	0
Myomyrus macrodon	0	0	0	1	0	0	0
Myomyrus macrops	0	0	0	1	0	0	0
Myomyrus pharao	0	0	0	1	0	0	0
Paramormyrops batesii	0	0	1	0	0	0	0

Species							
Paramormyrops curvifrons	0	0	1	0	0	0	0
Paramormyrops gabonensis	0	0	1	0	0	0	0
Paramormyrops hopkinsi	0	0	1	0	0	0	0
Paramormyrops kingsleyae	0	0	1	1	0	0	0
Paramormyrops longicaudatus	0	0	1	0	0	0	0
Paramormyrops ntotom	0	0	1	0	0	0	0
Paramormyrops taverneii	0	0	0	1	0	0	0
Petrocephalus arnegardi	0	0	0	1	0	0	0
Petrocephalus balayi	0	0	1	1	0	0	0
Petrocephalus binotatus	0	0	0	1	0	0	0
Petrocephalus boboto	0	0	0	1	0	0	0
Petrocephalus bovei	1	0	1	0	0	0	0
Petrocephalus catostoma	0	0	0	0	0	1	1
Petrocephalus christyi	0	0	1	1	0	0	0
Petrocephalus grandoculis	0	0	0	1	0	0	0
Petrocephalus levequei	0	1	0	0	0	0	0
Petrocephalus longicapitis	0	0	0	0	0	1	0
Petrocephalus magnitrunci	0	0	0	0	0	1	0
Petrocephalus magnoculis	0	0	0	0	0	1	0
Petrocephalus microphthalmus	0	0	1	1	0	0	0
Petrocephalus odzalaensis	0	0	0	1	0	0	0
Petrocephalus okavangensis	0	0	0	0	0	1	0
Petrocephalus pallidomaculatus	1	0	0	0	0	0	0
Petrocephalus pellegrini	1	1	0	0	0	0	0
Petrocephalus pulsivertens	0	0	0	1	0	0	0
Petrocephalus sauvagii	1	0	0	1	0	0	0
Petrocephalus schoutedeni	0	0	0	1	0	0	0
Petrocephalus soudanensis	1	0	0	0	0	0	0
Petrocephalus squalostoma	0	0	0	1	0	0	0
Petrocephalus sullivani	0	0	1	0	0	0	0
Petrocephalus tenuicauda	0	1	0	0	0	0	0
Petrocephalus valentini	0	0	0	1	0	0	0
Petrocephalus zakoni	0	0	0	1	0	0	0
Pollimyrus castelnaui	0	0	0	1	0	1	0
Pollimyrus isidori	1	0	0	0	0	0	0
Pollimyrus maculipinnis	0	0	0	1	0	0	0
Pollimyrus nigricans	0	0	0	1	0	0	1
Pollimyrus nigripinnis	0	0	0	1	0	0	0
Pollimyrus osborni	1	0	0	0	0	0	0
Pollimyrus pedunculatus	0	0	1	1	0	0	0
Pollimyrus petricolus	1	0	0	0	0	0	0
Pollimyrus plagiostoma	0	0	0	1	0	0	0
Pollimyrus pulverulentus	0	0	0	1	0	0	0
Pollimyrus schreyeni	0	0	0	1	0	0	0
Pollimyrus stappersii	0	0	0	1	0	0	0
Stomatorhinus fuliginosus	0	0	0	1	0	0	0
Stomatorhinus humilior	0	0	0	1	0	0	0
Stomatorhinus ivindoensis	0	0	1	0	0	0	0
Stomatorhinus kununguensis	0	0	0	1	0	0	0
Stomatorhinus microps	0	0	0	1	0	0	0
Stomatorhinus patrizii	0	0	0	1	0	0	0

Stomatorhinus polylepis	0	0	0	1	0	0	0
Stomatorhinus walkeri	0	0	1	0	0	0	0
Paramormyrops sphekodes	0	0	1	0	0	0	0

470

471

472

473

474

475

476

477

478

479

480

481

482

483

484

485

486

487

488

489

490

491   **Table S7**: Distribution of loci amongst the data subsets (SS1-SS10) and the complete data matrix

492   (SSAll) for 11 species with low assembly rates.

Taxa	SS1	SS2	SS3	SS4	SS5	SS6	SS7	SS8	SS9	SS10	SAll	%SAll
Kaupichthys hyporoides	6	6	1	5	5	3	4	2	1	2	35	6.6%
Gymnothorax reevesii	8	9	10	6	2	10	6	7	5	5	68	12.7%
Petrocephalus balayi	13	11	13	12	11	14	8	19	7	10	118	22.1%
Marcusenius sanagaensis	13	10	14	13	17	17	11	16	10	10	131	24.5%
Paramormyrops batesii	16	11	18	13	10	14	10	15	13	12	132	24.7%
Petrocephalus sp. 1	19	14	20	14	16	17	17	13	15	10	155	29.0%
Stomatorhinus fuliginosus	23	24	28	26	22	26	20	24	26	20	239	44.8%
Amia calva gill	26	35	26	26	16	32	24	26	26	24	261	48.9%
Papyrocranus congoensis	29	30	36	31	36	34	29	35	25	30	285	53.4%
Pantodon buchholzi	33	36	29	25	29	36	22	33	29	27	299	56.0%
Campylomormyrus compressirostris	31	37	33	30	27	36	24	31	27	24	300	56.2%

493

494

495

496

497

498

499

500

501

502

503

504

505

506

507   **Table S8:** Summary of support (AiC) and Log Likelihood (LnL) for 12 biogeographic models

508   optimized for two dispersal matrices (M0 and M1). The best fit model for each dispersal matrix

509   is bolded and the best fit model without the +J parameter is in blue. N = number of parameters; d

510   = dispersal; e = extinction, w = dispersal matrix power exponential; AICc Corrected Akaike

511   Information Criterion; AiCc weight = Ranked AICc models.

Schemes	LnL	N	d	e	j	w	AiCc	AiCc weight
M0								
DEC, see Fig. S5	**-320.3**	**2**	**0.012**	**2.00E-08**	**0**	**1**	**644.8**	**5.70E-06**
DEC+J	**-307.5**	**3**	**0.0094**	**1.00E-12**	**0.014**	**1**	**621.3**	**0.72**
DEC+W	-320.3	3	0.012	1.00E-12	0	0.0025	646.8	2.00E-06
DEC+J+W	-307.5	4	0.0094	1.00E-12	0.014	1.00E-05	623.4	0.25
DIVALIKE	-331.6	2	0.014	4.20E-09	0	1	667.3	7.40E-11
DIVALIKE+J	-320.3	3	0.011	1.00E-12	0.014	1	646.8	2.10E-06
DIVALIKE+W	-331.6	3	0.014	1.00E-12	0	0.0002	669.3	2.60E-11
DIVALIKE+J+W	-320.3	4	0.011	1.00E-12	0.014	0.016	648.9	7.30E-07
BAYAREALIKE	-365.8	2	0.013	0.078	0	1	735.8	9.90E-26
BAYAREALIKE+J	-311.1	3	0.0061	1.00E-07	0.026	1	628.3	0.021
BAYAREALIKE+W	-365.8	3	0.013	0.078	0	3.30E-05	737.8	3.50E-26
BAYAREALIKE+J+W	-311.1	4	0.0061	1.00E-07	0.026	0.017	630.4	0.0074
M1								
DEC	-309.9	2	0.021	0.0018	0	1	623.9	3.50E-05
DEC+J	-303.5	3	0.018	1.00E-12	0.014	1	613.1	0.008
DEC+W, see Fig. 4a	**-307.4**	**3**	**0.019**	**1.00E-12**	**0**	**0.26**	**621**	**0.0001**
DEC+J+W, see Fig. S4	**-297.6**	**4**	**0.015**	**1.00E-12**	**0.018**	**0.19**	**603.5**	**0.98**
DIVALIKE	-325.8	2	0.028	0.0087	0	1	655.7	4.50E-12
DIVALIKE+J	-320.6	3	0.023	0.0048	0.015	1	647.4	2.80E-10
DIVALIKE+W	-320.3	3	0.022	0.0006	0	0.18	646.8	3.80E-10
DIVALIKE+J+W	-310.7	4	0.017	1.00E-12	0.018	0.18	629.8	1.90E-06
BAYAREALIKE	-351	2	0.023	0.075	0	1	706	5.20E-23
BAYAREALIKE+J	-318.9	3	0.012	0.014	0.039	1	643.9	1.60E-09
BAYAREALIKE+W	-353.6	3	0.019	0.081	0	0.19	713.3	1.40E-24
BAYAREALIKE+J+W	-302.3	4	0.0089	1.00E-07	0.036	0.17	612.9	0.0086

512

513

514

515

516

517 **Table S9**: Comparison of ancestral ranges between range models and dispersal matrices for

518 select nodes in Mormyridae.

519

520

	MO		M1	
	DEC	DEC+*j*	DEC+*w*	DEC+*w+j*
MRCA Mormyridae	CB	CB	NSUG LGCB Z	CB
Ancestral Range of Tube Snouts				
Transitions 1 *Mormyrops caballus*, **Node: MRCA** *Mormyrops caballus* **and** *Mormyrops breviceps*	NSUG LGCB Z	NSUG LGCB Z	NSUG LGCB Z	NSUG LGCB Z
Transitions 2 *Mormyrops zanclirostris* **and** *Mormyrops boulengeri* **Node: MRCA** *Mormyrops zanclirostris* **and** *Mormyrops boulengeri*	CB	CB	CB	CB
Transitions 3 *Mormyrus caballus* **Node: MRCA** *Mormyrus ovis* **and** *Mormyrus caballus*	CB	CB	CB	CB
Transitions 4 *Mormyrus proboscirostris* **and** *Mormyrus rume* **Node: MCRA** *Mormyrus proboscirostris* **and** *Mormyrus rume*	NSUG LGCB	NSCB ECZ	NSUG LGCB	NSCB ECZ
Ancestral Range of Tube Snouts with Schaunzenorgan				
Transition 1 *Genyomyrus donnyi* **Node MRCA** *Genyomyrus donnyi* **and** *Gnathonemus echidnorhynchus*	CB	CB	CB	CB
Transitions 2 *Gnathonemus echidnorhynchus* **Node MRCA** *Gnathonemus echidnorhynchus* **and** *Marcusenius leopoldianus*	CB	CB	CB	CB
Transitions 3 *Campylomormyrus* **Node MRCA** *Campylomormyrus*	CB	CB	CB	CB

521

522

523

524

525

526

527

528

529

530

531   LIST OF APPENDICES

532

533   The Following data files are available on **Dryad** (link here):

534   **Appendix 1**: Alignments in nexus format. SSAll is the alignment with all exons, and SS1 – SS10

535   are the alignments for the 10 subsets of exons.

536   o   Alignment_SSAll.nexus

537   o   Alignment_SS1.nexus

538   o   Alignment_SS2.nexus

539   o   Alignment_SS3.nexus

540   o   Alignment_SS4.nexus

541   o   Alignment_SS5.nexus

542   o   Alignment_SS6.nexus

543   o   Alignment_SS7.nexus

544   o   Alignment_SS8.nexus

545   o   Alignment_SS9.nexus

546   o   Alignment_SS10.nexus

547   **Appendix 2:** Tree files (newick format) inferred for different subsets and methods (22

548   phylogenies estimated with IQ-Tree or Astral-III, 21-time calibrated trees using MCMCTree and

549   time-calibration tree with additional fossil calibration)

550   **Appendix 3:** R Scripts, code and input files for Ancestral State Estimation.

551   **Appendix 4:** R Scripts, code and input file for BioGeoBEARS.

552

553

554   LITERATURE CITED

555   Allen J.M., LaFrance R., Folk R.A., Johnson K.P., Guralnick R.P. 2018. aTRAM 2.0: An

556   Improved, Flexible Locus Assembler for NGS Data. Evol. Bioinforma. 14:0–3.

557   Arcila D., Ortí G., Vari R., Armbruster J.W., Stiassny M.L.J., Ko K.D., Sabaj M.H., Lundberg J.,

558   Revell L.J., Betancur-R. R. 2017. Genome-wide interrogation advances resolution of

559   recalcitrant groups in the tree of life. Nat. Ecol. Evol. 1:0020.

560   Arroyave J., Denton J.S.S., Stiassny M.L.J. 2020. Pattern and timing of diversification in the

561   African freshwater fish genus Distichodus (Characiformes: Distichodontidae). BMC Evol.

562   Biol. 20.

563   Betancur-R R., Wiley E.O., Arratia G., Acero A., Bailly N., Miya M., Lecointre G., Ortí G.

564   2017. Phylogenetic classification of bony fishes. BMC Evol. Biol. 17:162.

565   Black K.H., Archer M., Hand S.J., Godthelp H. 2012. The Rise of Australian Marsupials: A

566   Synopsis of Biostratigraphic, Phylogenetic, Palaeoecologic and Palaeobiogeographic

567   Understanding BT - Earth and Life: Global Biodiversity, Extinction Intervals and

568   Biogeographic Perturbations Through Time. In: Talent J.A., editor. Dordrecht: Springer

569   Netherlands. p. 983–1078.

570   Bolger A.M., Lohse M., Usadel B. 2014. Trimmomatic: A flexible trimmer for Illumina

571   sequence data. Bioinformatics. 30:2114–2120.

572   Bonde N. 2008. Osteoglossomorphs of the marine Lower Eocene of Denmark – with remarks on

573   other Eocene taxa and their importance for palaeobiogeography. Geol. Soc. London, Spec.

574   Publ. 295:253–310.

575   Brown B., Gaina C., Müller R.D. 2006. Circum-Antarctic palaeobathymetry: Illustrated

576   examples from Cenozoic to recent times. Palaeogeogr. Palaeoclimatol. Palaeoecol.

577   231:158–168.

578   Daniels S.R., Phiri E.E., Klaus S., Albrecht C., Cumberlidge N. 2015. Multilocus Phylogeny of

579   the Afrotropical Freshwater Crab Fauna Reveals Historical Drainage Connectivity and

580   Transoceanic Dispersal since the Eocene. Syst. Biol. 64:549–567.

581   Day J.J., Fages A., Brown K.J., Vreven E.J., Stiassny M.L.J., Bills R., Friel J.P., Rüber L. 2017.

582   Multiple independent colonizations into the Congo Basin during the continental radiation of

583   African Mastacembelus spiny eels. J. Biogeogr. 44:2308–2318.

584   Day J.J., Peart C.R., Brown K.J., Friel J.P., Bills R., Moritz T. 2013. Continental diversification

585   of an African catfish radiation (Mochokidae: Synodontis). Syst. Biol. 62:351–365.

586   Dupin J., Matzke N.J., Särkinen T., Knapp S., Olmstead R.G., Bohs L., Smith S.D. 2017.

587   Bayesian estimation of the global biogeographical history of the Solanaceae. J. Biogeogr.

588   44:887–899.

589   Flower B.P., Kennett J.P. 1994. The middle Miocene climatic transition: East Antarctic ice sheet

590   development, deep ocean circulation and global carbon cycling. Palaeogeogr.

591   Palaeoclimatol. Palaeoecol. 108:537–555.

592   Forey P.L., Hilton E. 2010. Two new Tertiary osteoglossid fishes (Teleostei:

593   Osteoglossomorpha) with notes on the history of the family. Morphol. phylogeny,

594   paleobiogeography Foss. fishes.:215–246.

595   Gill T. 1862. Description of a New Generic Type of Mormyroids and Note on the Arrangement

596   of the Genus. Proc. Acad. Nat. Sci. Philadelphia. 14:443–445.

597   Goodier S.A.M., Cotterill F.P.D., O'Ryan C., Skelton P.H., de Wit M.J. 2011. Cryptic diversity

598   of african tigerfish (genus hydrocynus) reveals palaeogeographic signatures of linked

599   neogene geotectonic events. PLoS One. 6.

600   Grabherr M.G.., Brian J. Haas, Moran Yassour Joshua Z. Levin, Dawn A. Thompson, Ido Amit,

601   Xian Adiconis, Lin Fan, Raktima Raychowdhury, Qiandong Zeng, Zehua Chen, Evan

602   Mauceli, Nir Hacohen, Andreas Gnirke, Nicholas Rhind, Federica di Palma, Bruce W. N.,

603   Friedman and A.R. 2013. Trinity: reconstructing a full-length transcriptome without a

604   genome from RNA-Seq data. Nat. Biotechnol. 29:644–652.

605   Greenwood P.H. 1972. New fish fossils from the Pliocene of Wadi Natrun, Egypt. J. Zool.:503–

606   519.

607   Hilton E.J. 2003. Comparative osteology and phylogenetic systematics of fossil and living bony-

608   tongue fishes (Actinopterygii, Teleostei, Osteoglossomorpha). :1–100.

609   Hilton E.J., Lavoué S. 2018. A review of the systematic biology of fossil and living bony-tongue

610   fishes, Osteoglossomorpha (Actinopterygii: Teleostei). Neotrop. Ichthyol. 16:1–35.

611   Hughes L.C., Ort G., Huang Y., Sun Y., Baldwin C.C., Thompson A.W., Betancur-R. R., Li C.,

612   Becker L., Zhao X., Li X., Fang C., Xie B., Zhou Z., Huang H., Chen S., Venkatesh B., Shi

613   Q. 2018. Comprehensive phylogeny of ray-finned fishes (Actinopterygii) based on

614   transcriptomic and genomic data. Procedings Natl. Acad. Sci.:2–7.

615   Hughes L.C., Ortí G., Saad H., Li C., White W.T., Baldwin C.C., Crandall K.A., Arcila D.,

616   Betancur-R R. 2020. Exon probe sets and bioinformatics pipelines for all levels of fish

617   phylogenomics. Mol. Ecol. Resour.:1–18.

618   Landis M.J., Matzke N.J., Moore B.R., Huelsenbeck J.P. 2013. Bayesian analysis of

619   biogeography when the number of areas is large. Syst. Biol. 62:789–804.

620   Lavier L.L., Steckler M.S., Brigaud F. 2001. Climatic and tectonic control on the Cenozoic

621   evolution of the West African margin. Mar. Geol. 178:63–80.

622   Lavoué S. 2016. Was Gondwanan breakup the cause of the intercontinental distribution of

623   Osteoglossiformes? A time-calibrated phylogenetic test combining molecular,

624   morphological, and paleontological evidence. Mol. Phylogenet. Evol. 99:34–43.

625 Lavoué S., Bigorne R., Lecointre G., Agnèse J.F. 2000. Phylogenetic relationships of mormyrid

626   electric fishes (Mormyridae; Teleostei) inferred from cytochrome b sequences. Mol.

627   Phylogenet. Evol. 14:1–10.

628 Lavoué S., Miya M., Arnegard M.E., Sullivan J.P., Hopkins C.D., Nishida M. 2012. Comparable

629   ages for the independent origins of electrogenesis in African and South American weakly

630   electric fishes. PLoS One. 7:1–18.

631 Lavoué S., Sullivan J.P. 2004. Simultaneous analysis of five molecular markers provides a well-

632   supported phylogenetic hypothesis for the living bony-tongue fishes (Osteoglossomorpha:

633   Teleostei). Mol. Phylogenet. Evol. 33:171–185.

634 Lévêque C., Oberdorff T., Paugy D., Stiassny M.L.J., Tedesco P.A. 2008. Global diversity of

635   fish (Pisces) in freshwater. Hydrobiologia. 595:545–567.

636 Li C., Hofreiter M., Straube N., Corrigan S., Naylor G.J.P. 2013. Capturing protein-coding genes

637   across highly divergent species. Biotechniques. 54:321–326.

638 Li H., Durbin R. 2009. Fast and accurate short read alignment with Burrows-Wheeler transform.

639   Bioinformatics. 25:1754–1760.

640 Li H., Handsaker B., Wysoker A., Fennell T., Ruan J., Homer N., Marth G., Abecasis G., Durbin

641   R. 2009. The Sequence Alignment/Map format and SAMtools. Bioinformatics. 25:2078–

642   2079.

643 Li W., Godzik A. 2006. Cd-hit: A fast program for clustering and comparing large sets of protein

644   or nucleotide sequences. Bioinformatics. 22:1658–1659.

645 Livingstone D.A., Rowland M., Bailey P.E. 1982. On the size of african riverine fish faunas.

646   Integr. Comp. Biol. 22:361–369.

647   Mai U., Mirarab S. 2018. TreeShrink: Fast and accurate detection of outlier long branches in

648   collections of phylogenetic trees. BMC Genomics. 19.

649   Matzke N.J. 2014. Model selection in historical biogeography reveals that founder-event

650   speciation is a crucial process in island clades. Syst. Biol. 63:951–970.

651   Montoya-Burgos J.I. 2003. Historical biogeography of the catfish genus Hypostomus

652   (Siluriformes: Loricariidae), with implications on the diversification of Neotropical

653   ichthyofauna. Mol. Ecol. 12:1855–1867.

654   Murray A.M., Wilson M.V.H. 2005. Description of a new Eocene osteoglossid fish and

655   additional information on †Singida jacksonoides Greenwood and Patterson, 1967

656   (Osteoglossomorpha), with an assessment of their phylogenetic relationships. Zool. J. Linn.

657   Soc. 144:213–228.

658   Murray A.M., Zelenitsky D.K., Brinkman D.B., Neuman A.G. 2018. Two new Palaeocene

659   osteoglossomorphs from Canada, with a reassessment of the relationships of the genus

660   Joffrichthys, and analysis of diversity from articulated versus microfossil material. Zool. J.

661   Linn. Soc. 183:907–944.

662   Pappenheim V.P. 1906. Neue und ungenügend bekannte elektrische Fische (Fam. Mormyridae)

663   aus den deutsch-afrikanischen Schutzgebieten. Sitzungsberichte der Gesellschaft

664   Naturforschender Freunde zu Berlin.:260–264.

665   Rambaut A., Drummond A.J., Xie D., Baele G., Suchard M.A. 2018. Posterior summarization in

666   Bayesian phylogenetics using Tracer 1.7. Syst. Biol. 67:901–904.

667   Ranwez V., Douzery E.J.P., Cambon C., Chantret N., Delsuc F. 2018. MACSE v2: Toolkit for

668   the alignment of coding sequences accounting for frameshifts and stop codons. Mol. Biol.

669   Evol. 35:2582–2584.

670 Ree R.H., Smith S.A. 2008. Maximum likelihood inference of geographic range evolution by

671   dispersal, local extinction, and cladogenesis. Syst. Biol. 57:4–14.

672 Rincon-Sandoval M., Duarte-Ribeiro E., Davis A.M., Santaquiteria A., Hughes L.C., Baldwin

673   C.C., Soto-Torres L., Acero P. A., Walker H.J., Carpenter K.E., Sheaves M., Ortí G., Arcila

674   D., Betancur-R R. 2020. Evolutionary determinism and convergence associated with water-

675   column transitions in marine fishes. "second Submiss. PNAS".:1–8.

676 Ronquist F. 1997. DISPERSAL-VICARIANCE ANALYSIS : A NEW APPROACH TO THE.

677   46:195–203.

678 Santaquiteria A., Siqueira A.C., Duarte-Ribeiro E., Carnevale G., White W., Pogonoski J.,

679   Baldwin C.C., Ortí G., Arcila D., Betancur-R. R. 2021. Phylogenomics and historical

680   biogeography of seahorses, dragonets, goatfishes, and allies (Teleostei: Syngnatharia):

681   assessing the factors driving uncertainty in biogeographic inferences. Syst. Biol.

682 Sepulchre P., Ramstein G., Fluteau F., Schuster M., Tiercelin J.J., Brunet M. 2006. Tectonic

683   uplift and Eastern Africa aridification. Science (80-.). 313:1419–1423.

684 Slater G.S.C., Birney E. 2005. Automated generation of heuristics for biological sequence

685   comparison. BMC Bioinformatics. 6:1–11.

686 Sullivan J.P., Lavoué S., Hopkins C.D. 2000. Molecular systematics of the African electric fishes

687   (Mormyroidea: teleostei) and a model for the evolution of their electric organs. J. Exp. Biol.

688   203:665–683.

689 Sullivan J.P., Lavoué S., Hopkins C.D. 2002. Discovery and phylogenetic analysis of a riverine

690   species flock of African electric fishes (Mormyridae: Teleostei). Evolution (N. Y). 56:597–

691   616.

692   Wheeler T.J., Eddy S.R. 2013. Nhmmer: DNA homology search with profile HMMs.

693   Bioinformatics. 29:2487–2489.

694   Wilson M.V.H., Murray A.M. 2008. Osteoglossomorpha: Phylogeny, biogeography, and fossil

695   record and the significance of key African and Chinese fossil taxa. Geol. Soc. Spec. Publ.

696   295:185–219.

697   Woodburne M.O., Case J.A. 1996. Dispersal, vicariance, and the Late Cretaceous to early

698   tertiary land mammal biogeography from South America to Australia. J. Mamm. Evol.

699   3:121–161.

700   Xu G.H., Chang M.M. 2009. Redescription of †paralycoptera wui Chang & Chou, 1977

701   (Teleostei: Osteoglossoidei) from the Early Cretaceous of eastern China. Zool. J. Linn. Soc.

702   157:83–106.

703   Zachos J., Pagani H., Sloan L., Thomas E., Billups K. 2001. Trends, rhythms, and aberrations in

704   global climate 65 Ma to present. Science (80-.). 292:686–693.

705   Zerbino D.R., Birney E. 2008. Velvet: Algorithms for de novo short read assembly using de

706   Bruijn graphs. Genome Res. 18:821–829.

707   Zhang J.-Y., Wilson M.V.H. 2017. First complete fossil Scleropages (Osteoglossomorpha).

708   Vertebr. Palasiat. 55:1–23.

709

710